Modeling of Oxygen Transport and Cell Killing in Type-II Photodynamic Therapy

Ioannis Gkigkitzis[1,2], Yuanming Feng[3,4], Chunmei Yang[4], Jun Q. Lu[1] and Xin-Hua Hu*[1]

[1]Department of Physics, East Carolina University, Greenville, NC
[2]Department of Mathematics, East Carolina University, Greenville, NC
[3]Department of Radiation Oncology, TJMUCH, Tianjin, China
[4]Department of Biomedical Engineering, Tianjin University, Tianjin, China

ABSTRACT

Photodynamic therapy (PDT) provides an effective option for treatment of tumors and other diseases in superficial tissues and attracts attention for *in vitro* study with cells. In this study, we present a significantly improved model of *in vitro* cell killing through Type-II PDT for simulation of the molecular interactions and cell killing in time domain in the presence of oxygen transport within a spherical cell. The self-consistency of the approach is examined by determination of conditions for obtaining positive definitive solutions of molecular concentrations. Decay constants of photosensitizers and unoxidized receptors are extracted as the key indices of molecular kinetics with different oxygen diffusion constants and permeability at the cell membrane. By coupling the molecular kinetics to cell killing, we develop a modeling method of PDT cytotoxicity caused by singlet oxygen and obtain the cell survival ratio as a function of light fluence or initial photosensitizer concentration with different photon density or irradiance of incident light and other parameters of oxygen transport. The results show that the present model of Type-II PDT yields a powerful tool to quantitate various events underlying PDT at the molecular and cellular levels and to interpret experimental results of *in vitro* cell studies.

INTRODUCTION

Photodynamic therapy (PDT) has been recognized as an effective option for treatment of cancers and other diseases (1,2). The therapeutic effects of PDT *in vivo* are realized through different mechanisms, which include direct killing of target cells, vascular shutdown and induction or modification of immune response. Therefore, investigations of PDT under *in vivo* conditions are critical to understand and improve clinical applications. On the other hand, *in vitro* studies of the very complex PDT processes with cultured cells have attracted significant attentions for multiple reasons (3–5). First, detailed study of PDT *in vitro* within a controlled cellular environment is essential to analyze the multiple signaling pathways underlying the cell killing effect of PDT. Second, cell killing through

PDT yields a unique case study of system biology in which cell repair and death in response to combined stimulations of photosensitizer and light can be quantitatively investigated and modeled. In response to treatment, cell death in a Type II PDT process can be initiated by production of singlet oxygen and other reactive oxygen species (ROS) with optically excited photosensitizers in the presence of oxygen molecules (6). In addition, oxygen functions as the essential molecules for cellular metabolism and other biochemical processes. Therefore, oxygen and associated transport play critical roles in the survival and death of PDT treated cells. Thus, a systematic study of oxygen transport in a single cell by taking into account of various molecular interactions and pathways can yield critical insights to understand the cytotoxicity and other effects of PDT.

Previously, we established a numerical model (7) to study the molecular interaction involved in Type-II PDT processes in time domain based on a method of rate equations proposed by Foster et al. (3,8,9). In that model, the concentrations of key molecules in both ground and excited states were solved as functions of illumination time with a group of coupled rate equations. By defining two decay constants to characterize the loss of ground-state photosensitizer and receptor oxidation, we have investigated the dependence of photobleaching and cytotoxicity on the initial concentrations of photosensitizer and incident light irradiance at the molecular level. The existing model, however, does not account for the oxygen transport inside and outside of the cell and provides no direct link to the observable cell survival curves. In this study, we present a significantly improved PDT model, which allows detailed examination of the roles played by oxygen and associated transport in a spherical cell configuration (10). Furthermore, this model includes a rate equation of cell killing *via* two molecular "death effectors" of single oxygen molecules or ROS and their receptors for calculation of cell survival ratio as a function of incident light fluence or initial photosensitizer concentrations. Numerical results are obtained with this model to demonstrate its utility for relating the cell survival curves to various parameters of molecular interactions that are critical to understand cell killing by PDT. As a result, the present model provides for the first time a powerful tool to quantitate the effects of oxygen in terms of cell survival curves that can be compared to the measured data.

MODELING METHODS

Rate equation group. A group of rate equations are used to quantitate the time evolution of the following molecule species in a Type-II PDT process: photosensitizers in the singlet ground state S_0; photosensitizers in the singlet and triplet excited states S_1 and T, respectively; oxygen molecules in triplet ground and singlet excited states $^3O_2$ and $^1O_2$; and unoxidized receptors R, which can be oxidized to induce cell killing (7). Even though the singlet excited oxygen molecules $^1O_2$ may play a critical role by themselves, it is well known that other ROS species are also involved in the cytotoxicity of PDT with mitochondria as the possible source and target sites (6). Consequently, the $^1O_2$ molecules here should be interpreted as the representatives of ROS molecules that include the singlet oxygen. Similar interpretation should also be made to the definition of receptors R, which symbolize the assembly of initiator and effector molecules inducing apoptosis, necrosis and autophagy in cells treated by PDT (11). With these guidelines in mind, we first employ six rate equations to describe the time evolution of the key molecular concentrations leading to the accumulation of oxidized receptors involved in the cytotoxicity through a Type-II PDT mechanism. These equations are given elsewhere to obtain a concentration vector of six components from $[S_0]$ to $[R]$ in the time domain

$$\frac{d[S_0]}{dt} = -k_{pb}[^1O_2][S_0] - v\rho\sigma_{psa}[S_0] + \frac{\eta_{10}}{\tau_1}[S_1] + \frac{\eta_{30}}{\tau_3}[T] + \frac{\alpha_s}{\tau_3}[T][^3O_2],$$
(1)

$$\frac{d[S_1]}{dt} = -\frac{1}{\tau_1}[S_1] + v\rho\sigma_{psa}[S_0],$$
(2)

$$\frac{d[T]}{dt} = -\frac{\eta_{30}}{\tau_3}[T] - \frac{\alpha_s}{\tau_3}[T][^3O_2] + \frac{\eta_{13}}{\tau_1}[S_1],$$
(3)

$$\frac{\partial[^3O_2]}{\partial t} = -\frac{\alpha_s}{\tau_3}[T][^3O_2] + \frac{\eta_o}{\tau_o}[^1O_2] + D\nabla^2[^3O_2] - \frac{V_m[^3O_2]}{[^3O_2] + K_m},$$
(4)

$$\frac{d[^1O_2]}{dt} = -k_{pb}[S_0][^1O_2] - k_{cx}[R][^1O_2] - \frac{\eta_o}{\tau_o}[^1O_2]$$
$$+ \frac{\alpha_s}{\tau_3}[T][^3O_2] - k_{sc}[C]_i[^1O_2],$$
(5)

$$\frac{d[R]}{dt} = -k_{cx}[^1O_2][R] + U.$$
(6)

The definitions of coefficients and their values used in the above equations have been detailed in (7) and are provided in the Appendix for completeness. The initial conditions of Eqs. (1–6) at the beginning of illumination ($t = 0$) are given by an initial concentration vector of $([S_0]_i, 0, 0, [^3O_2]_i, 0, [R]_i)$ and the spatial variation of the oxygen concentration is limited to the interior of a cell, *i.e.* $0 \le r < r_0$, with r_0 as the radius of the spherical cell. The second term U on the right-hand side of Eq. (6) is set to be a very small positive constant at $1(cm^{-3} s^{-1})$ for avoiding appearance of negative concentrations in numerical calculations as to be discussed later. It is verified that the small valued U has no effect on calculations of decay constants and cell survival ratio.

For the six equations listed elsewhere, the first three and last two remain essentially the same as presented in our previous model (7) except the repair term U in Eq. (6). In these equations, we do not consider the spatial dependence of molecular concentrations for two reasons. First, the molecules of photosensitizers and receptors are much larger and more massive than the small oxygen molecules and therefore the associated diffusions take a much longer time to become significant in PDT process. This argument should also apply to the excited photosensitizers T acting as a substrate for transferring energy from photons to oxygen molecules with a relaxation time τ_3. Second, the highly active molecules of S_1 and $^1O_2$ have very fast relaxation rates to ground states. Consequently, their respective relaxation times of τ_1 and τ_0 were chosen as 10 and 30 (ns) in our previous study, which are much smaller than τ_3 ($= 30 [\mu s]$) and thus prevent the molecules from diffusing into locations other than the immediate neighboring sites (7). Next, we will consider Eq. (4), which contains a term on the diffusion of the ground-state oxygen molecules $^3O_2$.

Oxygen diffusion and boundary conditions. Diffusion of $^3O_2$ in cells has attracted research interests in consideration of cellular metabolism and other biochemical processes. Quantitative modeling has been pursued in a spherical configuration in which a spherical symmetry of oxygen distribution or $[^3O_2](\mathbf{r}) = [^3O_2](r)$ was assumed to simplify mathematical treatment. With this model one considers the rate of oxygen uptake by molecules in the metabolism and processes unrelated to PDT using a nonlinear Michaelis–Menten term of two adjustable parameters (12): V_m represents the maximum rate of oxygen uptake as $[^3O_2] \rightarrow \infty$ while K_m yields the value of $[^3O_2]$ for the Michaelis–Menten term to reach a half-maximum uptake rate. We adopt this spherical cell configuration to study oxygen diffusion in a Type-II PDT process using Eq. (4). To establish an appropriate boundary-value problem related to oxygen diffusion, boundary conditions at the cell center ($r = 0$) and membrane ($r = r_0$; 12) are introduced in the following to complement the Eq. (4)

$$\begin{cases} \frac{\partial[^3O_2]}{\partial r} = 0, & if \ r = 0 \\ D\frac{\partial[^3O_2]}{\partial r} = M\{[^3O_2]' - [^3O_2]\}, & if \ r = r_0 \end{cases}$$
(7)

where M is the parameters of oxygen permeability and $[^3O_2]'$ refers to the outside concentration.

If $[^3O_2]'$ distributes outside the cell according to a homogeneous diffusion process with D' as the extracellular diffusion constant, one can show that Eq. (7) can be further simplified to the following:

$$\begin{cases} \frac{\partial[^3O_2]}{\partial r} = 0, & if \ r = 0 \\ D\frac{\partial[^3O_2]}{\partial r} = M\{1 - \frac{Mr_0}{D'+Mr_0}\}\{[^3O_2]_i - [^3O_2]\}, & if \ r = r_0 \end{cases}$$
(8)

where we assumed $[^3O_2]_\infty = [^3O_2]_i$ as the oxygen concentration far from the cell. In this study, the permeability M is used as one of the adjustable parameters to account for the variation of topology of cell membrane due to the presence of microvilli and ruffles. For example, it has been suggested that ruffled cell membrane can reduce its permeability to oxygen because of extended area using a 2D random walk model (13). For results presented here, we vary the parameter M from a "classical" value of 2×10^{-2} (cm s^{-1}; 14) to 2×10^{-5} (cm s^{-1}) to allow a detailed study of oxygen permeability across the cell membrane. Figure 1 illustrates schematically various molecular reactions and processes involved in a Type-II PDT considered here with the coefficients and parameters characterizing the interactions and oxygen transport in a spherical cell.

Decay constants of photosensitizer and receptor concentrations. The group of differential equations from (1–6) can be solved numerically in time domains under the boundary conditions of Eq. (8) to obtain a solution vector of six molecular concentrations. The effects of oxygen diffusion within the cell and across the membrane on the solution vector of concentrations are investigated with this model for quantitative understanding of the molecular kinetics related to the Type-II PDT. We use the partial differential equation (PDE) solver (pdepe) by MATLAB (The MathWorks, Natick, MA) to obtain the solution vector as a function of illumination time t from the start of illumination at $t = 0$ to 3000 (s). Two components of the solution vector, $[S_0]$ and $[R]$, are of particularly interest to our study whose concentration and time dependences can be used to quantitate the phenomena of photobleaching and cytotoxicity in a Type-II PDT process. Consequently we define two decay constants of t_S and t_R for characterization of the initial decrease of $[S_0]$ and $[R]$, respectively, caused by photon absorption (7). Utilization of t_S and t_R allows detailed mapping of these decay constants on the grid of the two key parameters: photon density ρ proportional to the incident light irradiance and the initial photosensitizer concentration $[S_0]_i$ for inducing cytotoxicity. Effects of other parameters are studied by mapping the two decay constants at different values of the oxygen diffusion constants D and D', the membrane permeability M and the maximum rate of oxygen uptake V_m.

Cell killing model. The equation group from (1–6) can be solved to characterize the main molecular interaction involved in Type-II PDT. Although some of the molecular concentrations are measurable such as $[S_0]$ and $[^3O_2]$, experimental verification of these quantities can be difficult, if not impossible and they relate indirectly to the ultimate consequence of PDT for cell killing. It is thus highly desired to develop a cell killing model that can link the molecular concentrations to the cell survival ratio, which can be measured with an *in vitro* cell model. We
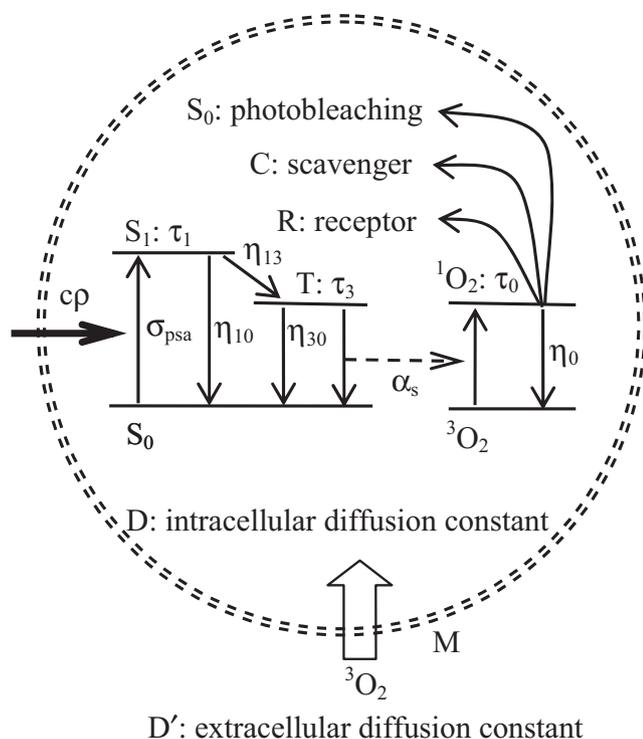
Figure 1. A schematic diagram to illustrate the molecular interaction and diffusion in a spherical cell model.

mainly consider two forms of cytotoxicity related to PDT induced by ROS. One is due to the accumulation of oxidized receptors for initiation of apoptosis with the rate of cell killing linearly proportional to the concentration of oxidized receptors (15). Another is described by a nonlinear term similar to the Michaelis–Menten terms used in Eq. (4), which represents the receptor-independent contributions to the rate of cell killing as a result of ROS stress (16). This term becomes significant as the concentration of $^1O_2$ or ROS becomes large relative to K_c. The nonlinear term therefore allows the inclusion of the coefficient K_c to simulate the effect of cell repair. We include these two terms into the following equation to quantitate the PDT cytotoxicity as:

$$\frac{dN}{d} = -\beta_0(1 - \frac{[R]}{[R]_i})N - \frac{V_c[^1O_2]}{[^1O_2] + K_c} \tag{9}$$

where N can be interpreted as either the cell survival ratio or probability of cell survival with the initial condition given by $N(0) = 1$, the coefficients of β_0 and V_c are parameters that can be adjusted to vary the weights of the two terms and K_c is used for characterization of the cell's ability to resist or repair damage by ROS. The values of these coefficients are given in the Appendix for results presented elsewhere. The above equation can be solved simultaneously with equations of (1–6) under the boundary condition of Eq. (8) to obtain the cell survival ratio N as a function of incident light fluence F. The fluence F is obtained from the illumination time t and the irradiance of incident light or the photon density ρ as the form $F \propto \rho t$.

Positive definite test of the solution vector in time domain. Equations (1–6) form a system of parabolic PDEs with the boundary condition defined in Eq. (8). It is therefore of interest to inquire under what conditions the equation group could produce a solution vector of positive definite components to be consistent with their definitions. To derive these conditions, we employ a strong maximum principle recently proved for parabolic PDE (17). Each of Eqs. (1–3) and Eqs. (5) and (6) in the group can be casted into a parabolic PDE form like Eq. (4) if we add a Laplace term with a positive diffusion constant of negligibly small value ($= 1 \times 10^{-15}$ [cm^2 s^{-1}]). This allows us to use Eq. (4) as an example for application of the strong maximum principle by replacing $[^3O_2]$ with a function $f(r, t)$, which is assumed to be continuous over the domain of ($0 \leq r < r_0, 0 \leq t$). We first rearrange Eq. (4) into the following form

$$\frac{\partial f}{\partial t} - D\nabla^2 f + (\frac{V_m}{f + K_m} + \frac{\alpha_s}{\tau_3}[T])f - \frac{\eta_o}{\tau_o}[^1O_2] = 0. \tag{10}$$

If $\frac{\eta_o}{\tau_o}[^1O_2] \geq 0$, then the above equation can be turned into an inequality as

$$\frac{\partial f}{\partial t} - D\nabla^2 f + \gamma f \geq 0. \tag{11}$$

where $\gamma(r, t) = \frac{V_m}{f + K_m} + \frac{\alpha_s}{\tau_3}[T]$. The strong maximum principle applies to the above inequality if D and γ are locally bounded and $\gamma > 0$, which yields the following conclusion (17): $f(r, t) = 0$ for all $t < t_0$ if $f(r, t) = 0$ at $t = t_0$. According to this result a molecular concentration $f(r, t)$ remains positive once it becomes positive as long as the following two conditions are satisfied: (1) other coupling molecular concentrations (such as $[^1O_2]$) stay positive to ensure that Eq. (10) can be converted into the inequality (11); and (2) the coefficient γ is positive. A quick examination shows that each of the Eqs. (1–6) can be converted into the form of inequality (11) and both conditions can be satisfied if the concentrations of the coupling molecules are initially positive or become positive after $t = 0$. One should note that the strong maximum principle applies only to the open domain of the spatial variable r ($0 \leq r < r_0$; 17). At the boundary of spatial domain $r = r_0$, a molecular concentration is not prohibited to become negative.

RESULTS AND DISCUSSION

Time-domain results during light illumination for the molecular concentrations

We solve the boundary-value problems of molecular concentrations defined by the group of Eqs. (1–6) under the boundary condition of Eq. (8) in the time domain from $t = 0$ to 3000 (s) with 1000 steps on a logarithmic scale to reduce numerical errors. The spatial domain between the cell center at $r = 0$ to the membrane boundary at $r_0 = 5$ (μm) is divided into a linear mesh of either 10- or 40-step. Figure 2 presents the time dependence of six normalized molecular concentrations calculated with the 40-step spatial mesh with the oxygen diffusion shut off by using negligible diffusion constants of D and D'. The concentrations are plotted against the illumination time t in two groups: the ground-state molecules of $[S_0]$, $[^3O_2]$ and $[R]$ and the excited ones of $[S_1]$, $[T]$ and $[^1O_2]$. Three intracellular locations are chosen to exhibit the spatial variation of concentrations. The lack of oxygen diffusion requires the use of high initial oxygen concentration at $[^3O_2]_i = 5.0 \times 10^{17}$ (cm^{-3}) to observe significant decay of $[S_0]$ and $[R]$ for $t \leq 3000$ (s). It can be seen easily from the result presented in Fig. 2 that the lack of oxygen leads to progressively severe hypoxia for locations away from the cell boundary at $r = r_0$. This in turn affects the production of singlet oxygen so that the maximum values of $[^1O_2]$ decrease from 85.2% at $r = 0.975r_0$ to 24.9% at $r = 0$ in comparison to the maximum $[^1O_2]$ at the boundary of $r = r_0$. Similarly, the decrease of the unoxidized receptor concentration $[R]$ becomes less steep as one moves toward the cell center at $r = 0$. It can also be seen that the changes of $[^1O_2]$ among the three locations for the time period from 100 to 1000 (s) show different variations. The two intracellular locations as shown in Fig. 2(b) and (d) show initial reductions of $[^1O_2]$ followed by increases, whereas near the cell boundary in Fig. 2(f) $[^1O_2]$ increases are rapidly followed by a drop. From the time dependences of $[^3O_2]$, $[S_0]$ and $[R]$ and Eq. (5), one can observe that the intracellular $[^1O_2]$ is dominated by the changes in $[^3O_2]$ for poor transport, whereas the variation at
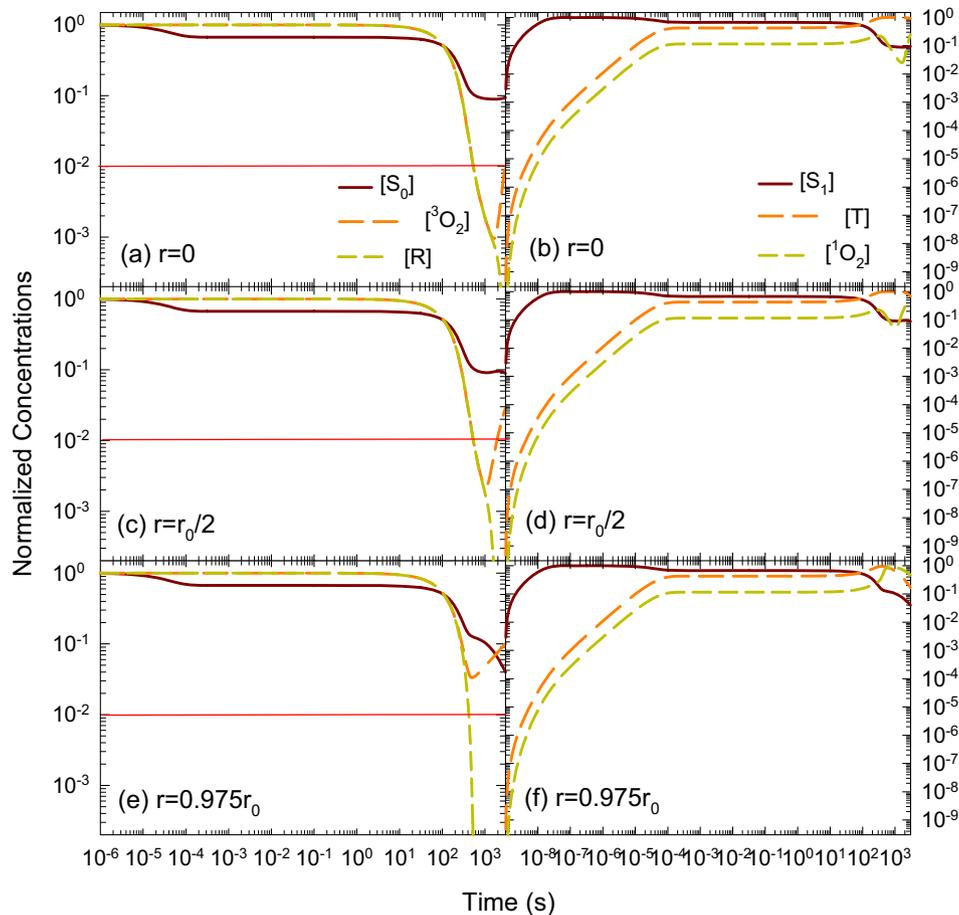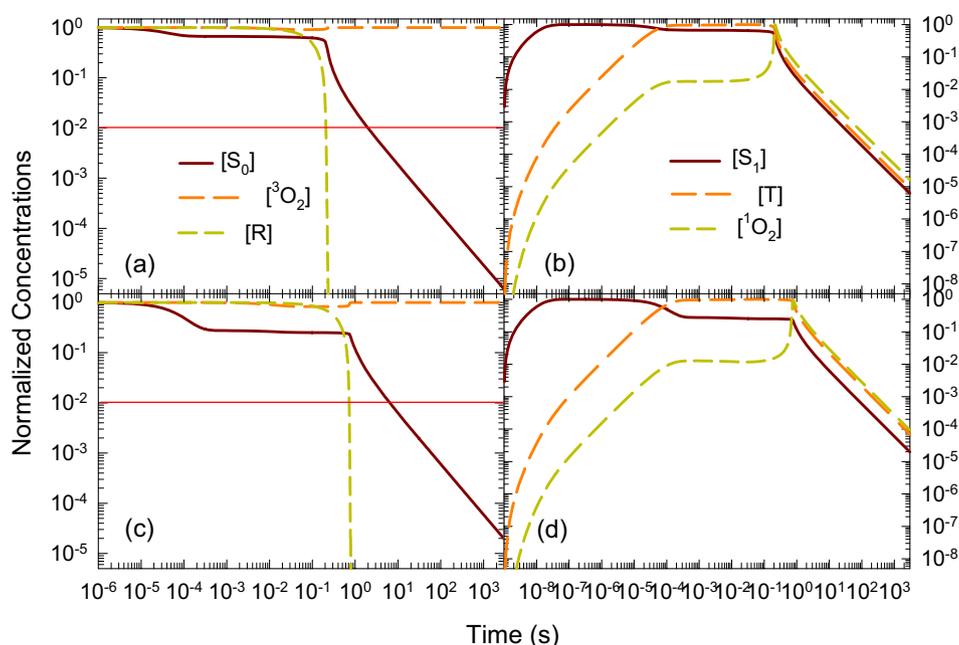
Figure 2. Time dependence of the solution vector at three intracellular locations using a 40-step spatial mesh and illumination starting at $t = 0$: (a), (c) and (e): concentrations of ground-state molecules normalized by their initial values; (b), (d) and (f): concentrations of excited molecules normalized by their maximum values on the spatial mesh. The values of the parameters are given by: $\rho = 1 \times 10^6$ (cm^{-3}), $[S_0]_i = 5.00 \times 10^{11}$ (cm^{-3}), $D = 8.00 \times 10^{-12}$ (cm^2 s^{-1}), $D' = 2.00 \times 10^{-12}$ (cm^2 s^{-1}), $M = 2.00 \times 10^{-2}$ (cm s^{-1}), $[^3O_2]_i = 5.06 \times 10^{17}$ (cm^{-3}), $V_m = 0$. The values of other coefficients are given in the Appendix and the red lines indicate the thresholds for the decay constants.

the boundary is due to consumption of single oxygen that includes photobleaching. By raising the oxygen diffusion constants toward 10^{-5} to 10^{-6} (cm^2 s^1), the intracellular heterogeneity of oxygen distribution starts to disappear as confirmed by the results calculated at different locations (not shown here). We point out that all of the concentration values shown in Fig. 2 and other similar results remain positive, as expected based on the strong maximum principle.

We have calculated the molecular concentrations at the boundary of $r = r_0$ obtained with different spatial meshes of 40- and 10-step to increase simulation speed. The values of $[R]$ indeed become negative at the cell boundary for $[R]$ at $t \sim 500$ (s) for both spatial meshes. By increasing the spatial mesh density or the step number from 10 to 40, the number of negative $[R]$ values; however, can be reduced from 20 to 7 among the 1000 data points in the time domain. In all cases the magnitude of negative $[R]$ values are less than 10^{-3} of its initial value. These results (not shown) suggest that the negative $[R]$ calculated from the boundary-value problem defined here can be attributed to the numerical rounding errors. Furthermore, the appearance of small negative values of $[R]$ does not affect our calculation of the decay constant

and use of 10-step mesh can significantly reduce computation time with little reduction in accuracy. Consequently, we adopt the 10-step mesh for the calculation of decay constants presented elsewhere.

To illustrate the effect of diffusion, we show in Fig. 3 the time-domain data with diffusion constants typically used in previous studies of oxygen diffusion (14, 18). For these high values of D and D', sufficient oxygen is supplied through diffusion so the time evolution of the concentration vector is nearly independent of spatial location. Consequently, Fig. 3 presents only the results calculated at the middle location of the spherical cell. Because of the efficient diffusion, the influence of initial oxygen concentration $[^3O_2]_i$ is much reduced. In the previous study, we proved that the time evolution and decay constants of $[S_0]$ and $[R]$ are very sensitive to the values of $[^3O_2]_i$ without consideration of oxygen diffusion, as shown by Figs. 4 and 5 in (7). Those data are significantly different from the results presented in Fig. 3 in which a large difference in $[^3O_2]_i$ leads to similar time evolution of molecular concentrations. Nevertheless, $[^3O_2]_i$ can affect the levels of $[^1O_2]$ and subsequently the cell survival ratio as described by Eq. (9).

Figure 3. Time dependence of the solution vector at the middle of the cell ($r = r_0/2$) using the 40-step mesh and $D = 8.00 \times 10^{-6}$ (cm^2 s^{-1}) and $D' = 2.00 \times 10^{-5}$ (cm^2 s^{-1}) for different initial oxygen concentration: (a) and (b): $[^3O_2]_i = 5.0 \times 10^{17}$ (cm^{-3}); (c) and (d): $[^3O_2]_i = 7.0 \times 10^{16}$ (cm^{-3}). All other coefficients are of the same values as those in Fig. 2.
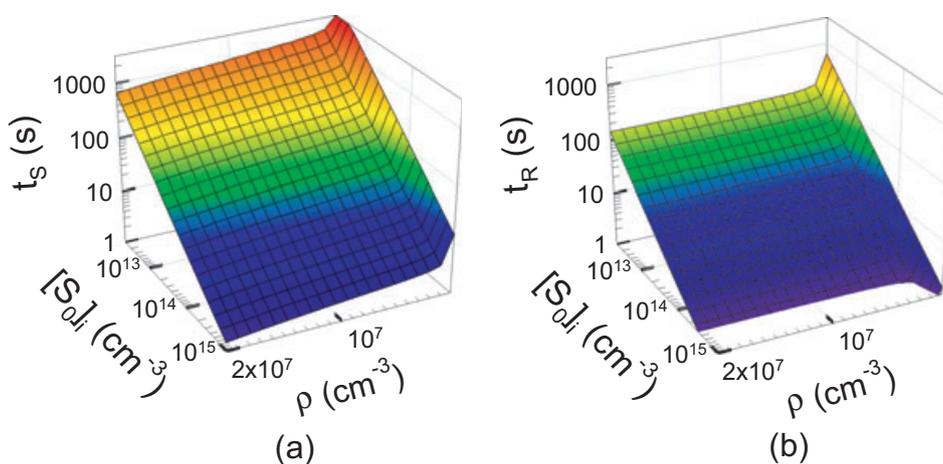
Figure 4. The decay constants of (a) t_S and (b) t_R *versus* the initial photosensitizer concentration $[S_0]_i$ and photon density ρ at the cell center ($r = 0$). The values of parameters are given by $D = 8 \times 10^{-6}$ (cm^2 s^{-1}), $D' = 2 \times 10^{-5}$ (cm^2 s^{-1}), $M = 2.00 \times 10^{-2}$ (cm s^{-1}), $[^3O_2]_i = 7.00 \times 10^{16}$ and $V_m = 2.9 \times 10^{18}$ (cm^{-3} s^{-1}) with all other coefficients given in the Appendix.

Mapping of decay constants on the mesh of $[S_0]_i$ and ρ

As can be seen from the results in Figs. 2 and 3, the time evolutions of photosensitizer concentration $[S_0]$ and unoxidized receptor concentration $[R]$ are often dominated by steep reduction with increasing time of illumination. This prompts us to define two decay constants of t_S and t_R to characterize efficiently the two key processes in the Type-II PDT at the molecular level: photobleaching related to $[S_0]$ and cytotoxicity related to $[R]$. The group of Eqs. (1–6) is solved in time domain to obtain t_S and t_R as the times for $[S_0]$ and $[R]$ to be reduced to 1% of their initial values at various values of the initial photosensitizer concentration $[S_0]_i$ and photon density ρ. The time-domain calculations and extraction of t_S and t_R are iterated

on a 20×20 semi-log mesh of $[S_0]_i$ and ρ with $[S_0]_i$ ranging from 2.0×10^{12} to 1.0×10^{15} (cm^{-3}) and ρ ranging from 1.0×10^{5} to 2.0×10^{7} (cm^{-3}). The maximum values of the chosen ranges correspond respectively to about 5 (μg mL^{-1}) for Photofrin$^{®}$ used as photosensitizer and about 80 (mW cm^{-2}) for the incident light irradiance as it relates to ρ (7). Different values of the oxygen diffusion constants, permeability and strength of the Michaelis–Menten term parameters are employed for the time-domain calculations carried out at two locations of cell center ($r = 0$) and boundary ($r = r_0$). As a reference, Fig. 4 presents the results of decay constants obtained with $D = 8.0 \times 10^{-6}$ (cm^2 s^{-1}), $D' = 2.0 \times 10^{-5}$ (cm^2 s^{-1}), $M = 2.0 \times 10^{-2}$ (cm s^{-1}) and $V_m = 2.9 \times 10^{18}$ (cm^{-3} s^{-1}) based on previous reports (14) with a low-initial oxygen concentration of $[^3O_2]_i = 7.0 \times 10^{16}$

(cm^{-3}). As t_S and t_R exhibit similar dependences on $[S_0]_i$ and ρ among all three cell locations, only those at the cell center of $r = 0$ are presented in Fig. 4. In contrast, the mapping of decay constants are presented in Figs. 5 and 6 at both cell center and boundary with different values of D, D', $[^3O_2]_i$ and M.

The results presented in Figs. 4–6 demonstrate the utility of the modeling tool developed here, which makes it possible to quantitatively investigate and compare the different effects on the molecular aspects of PDT by variation of parameters related to the supply and consumption of oxygen. We examine the mapping results without the presence of additional oxygen consumption described by the Michaelis–Menten term by setting $V_m = 0$ and find no significant changes from the results in Fig. 4. It appears that the oxygen consumption *via* metabolism has limited effect on the decay of $[S_0]$ and $[R]$ in PDT for the V_m used and causes no significant differences among the decay constants calculated at different cellular locations. We also observe that for the ranges of $[S_0]_i$ and ρ chosen the decay constants are of much higher sensitivity to $[S_0]_i$ than that to ρ, which indicates sufficient supplies of photons and oxygen. With the Michaelis–Menten term, we further examine the effect of oxygen diffusion by reduction of the diffusion constants by 10-fold and the permeability by 1000-fold. These variations lead to observable changes of the decay constants at different cell locations as shown in Figs. 5 and 6. It is interesting to note that the weakened oxygen transport can cause faster photobleaching, but slower oxidization of the receptors R at the cell center than those at the boundary as the photon density or incident light irradiance is increased.

The cell survival curves

Accurate modeling of cell killing by PDT remains a challenging task because of the complexity of the process. As our first effort toward a full solution, the group of Eqs. (1–6) and (9) are solved under the boundary conditions described by Eq. (8) to obtain the cell survival ratio or probability N as a function of illuminating time t. The solution is then converted into a function of incident light fluence, $N(F)$, by converting t into light fluence as $F = 4 \times 10^{-9}\rho t$ in the unit of (J cm^{-2}) with ρ and t taking the unit of (cm^{-3}) and (s), respectively (7). After detailed analysis of the results calculated with different coefficients used in Eq. (9), we chose the values of β_0, V_c and K_c as given in the Appendix to obtain numerical results that are comparable to the measured data published by other researchers (3–5). Figure 7 presents typical results of cell survival curves obtained with $\beta_0 = 1.0 \times 10^{-2}$ (s^{-1}) and different values of ρ, $[S_0]_i$, $[^3O_2]_i$, D, D' and M. Each set of curves consists of triplicate lines calculated at three spatial locations of cell center, middle and boundary with each assumed to be the targeted sites of PDT cytotoxicity. The cell
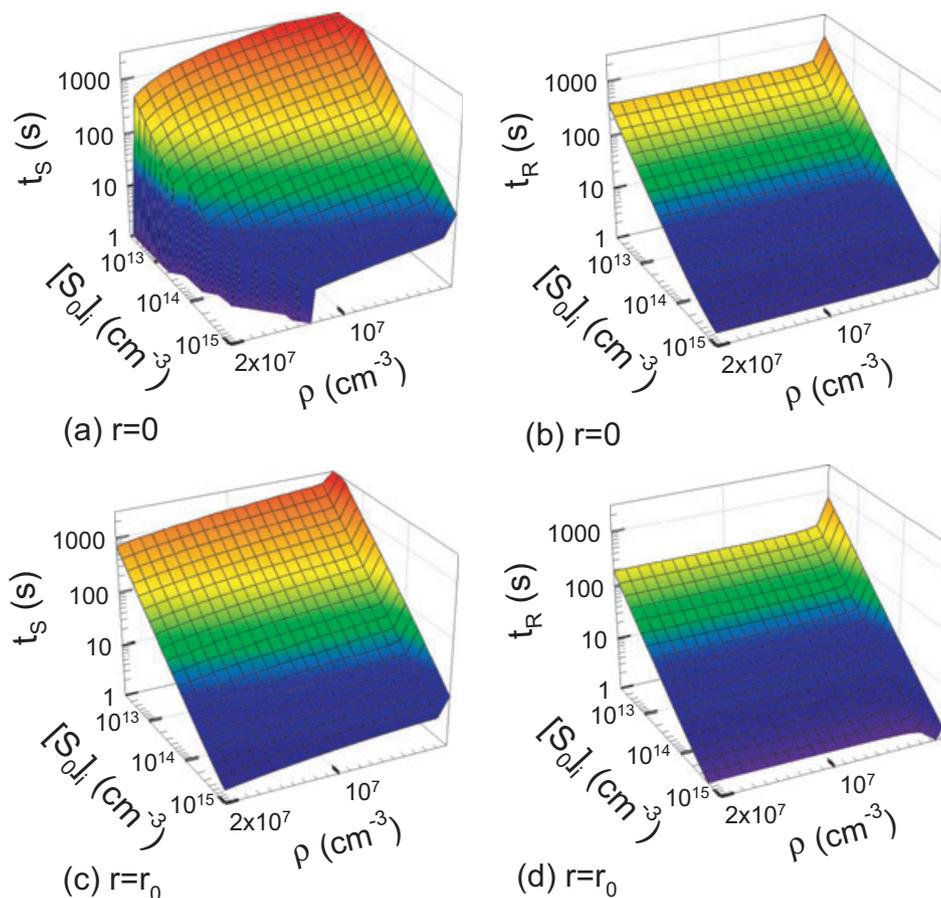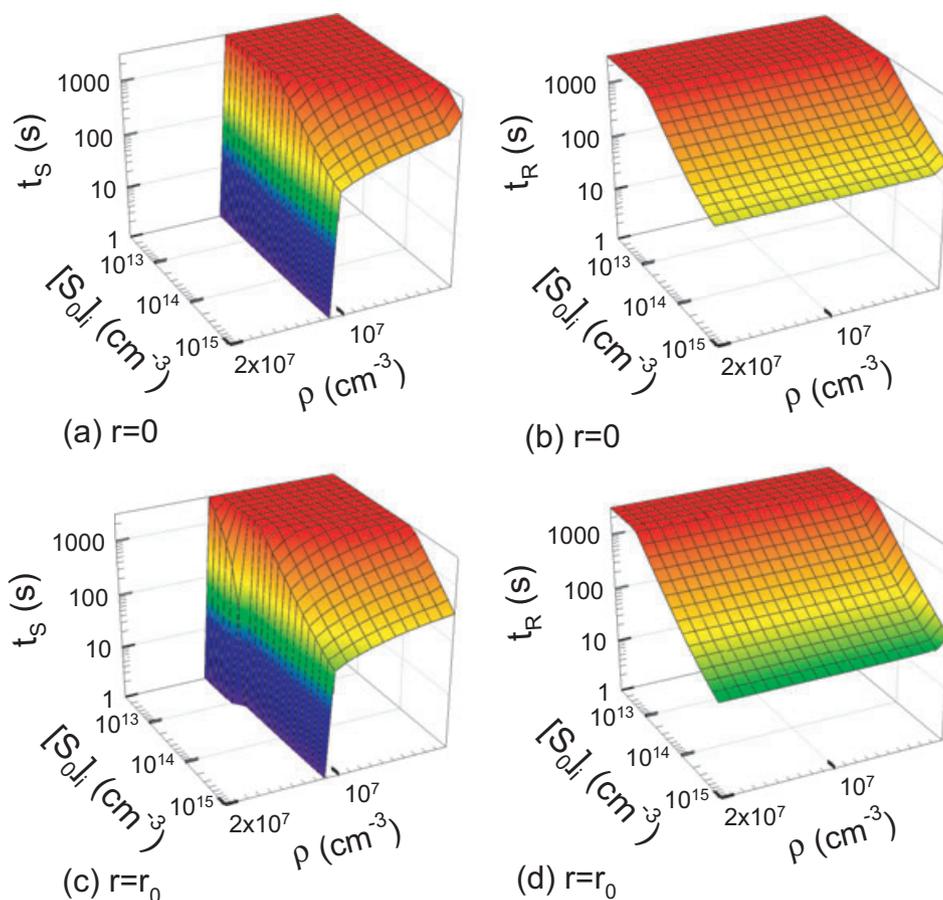

Figure 5. The decay constants of t_S and t_R *versus* the initial photosensitizer concentration $[S_0]_i$ and photon density ρ at the cell center ($r = 0$) for (a) and (b); at the cell boundary ($r = r_0$) for (c) and (d). The values of other parameters and coefficients are the same as those in Fig. 4 except the following: $D = 8.0 \times 10^{-7}$ (cm^2 s) and $D' = 2.0 \times 10^{-6}$ (cm^2 s^{-1}).

survival curves presented in Fig. 7 can be divided into two parts that relate separately to the two terms on the right-hand side of Eq. (9). The first term is linearly proportional to [R] and determines the slope of the initial exponential decrease of N for small F. As F rises, the second term related to [$^1O_2$] concentration or ROS stress starts to contribute significantly to the killing rate and causes an accelerated drop of the survival curve.

From Fig. 7(a) to (d), we show in each diagram three sets of curves calculated at different photon density values with different parameters of initial oxygen concentration and diffusion constants. It is clear from these results that increasing photon density leads to increasing survival ratio at the same fluence, which is widely known in the cell study of PDT as a result of poor oxygen supply for illumination at high irradiance (3–5). The effect of poor oxygen supply or hypoxia can be further seen by comparing Fig. 7(b) to (a) where [$^3O_2$]$_i$ is reduced by a factor of 100 to yield significant enhancement of cell survival. The oxygen diffusion constants and permeability also influence cell survival as demonstrated in Fig. 7(c) and (d) in which D, D′ and M are reduced. These results show higher cell survival ratios correlate to weakened oxygen diffusion and variation of cell killing among cells with different target site locations due to spatial heterogeneity in oxygen distribution. Finally, Fig. 7(e) and (f) present the modeling results using different initial photosensitizer concentrations and diffusion constants. Fig. 7(a) reveals that increasing [S_0]$_i$ leads to

reduced cell survival as expected. A 142-fold increase in the supply of [S_0]$_i$ is not accompanied by a similarly enhanced cell killing as demonstrated by the relatively small difference between the two sets of curves labeled with [S_0]$_{i1}$ and [S_0]$_{i2}$ in Fig. 7(e). The reduced oxygen diffusion in Fig. 7(f) exhibits marked difference among the triplicate lines obtained at different cell locations, especially for the low value of [S_0]$_i$ at [S_0]$_{i3}$, which indicates a strong competition for oxygen between the cytotoxicity of PDT and unrelated metabolism processes represented by the Michaelis–Menten term in Eq. (4).

To further demonstrate the utility of the PDT model presented here, we show in Fig. 8 a comparison of our numerical results with the experimental data reported by Qin et al., which were obtained with lymphoma cells treated by Photofrin®-PDT (5). The laser irradiance at the wavelength of 635 nm was varied to adjust fluence with a fixed illumination time of 30 (s). Fig. 8 replots the cell survival data measured by the clonogenic assay method as presented in fig. 3B of (5). We carry out time domain calculations with $0 < t \leq 30$ (s) at three cell locations and plot N ($t = 30$ s) versus [S_0]$_i$ as two sets of survival curves in Fig. 8. The two different values of photon density ρ used for the numerical results are based on the fluence values of $F = 75$ and 300 (mJ cm^{-2}) as reported in (5). As can be seen from Fig. 8, the present PDT model agrees reasonably well with the measured cell survival data for the case of high fluence at $F = 300$ (mJ cm^{-2}) by adjusting the

Figure 6. The decay constants of t_S and t_R versus the initial photosensitizer concentration [S_0]$_i$ and photon density ρ at the cell center ($r = 0$) for (a) and (b); at the cell boundary ($r = r_0$) for (c) and (d). The values of other parameters and coefficients are the same as those in Fig. 5 except the following: $M = 2.00 \times 10^{-5}$ (cm s^{-1}).
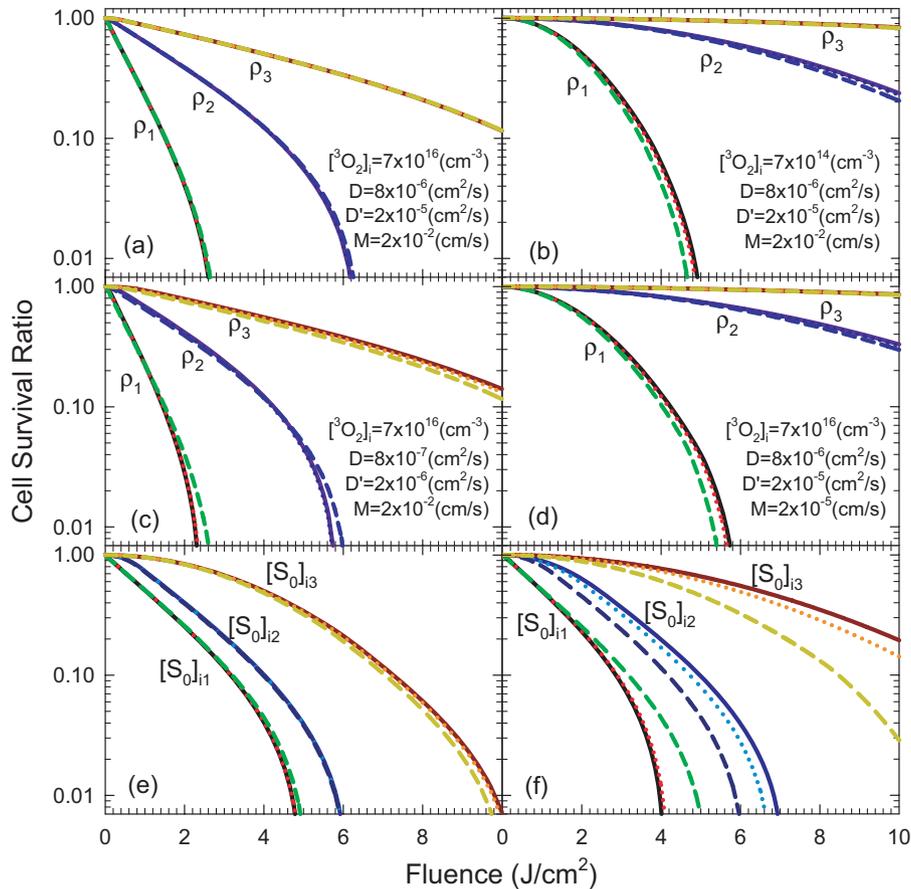
Figure 7. The cell survival ratio curves calculated with $V_m = 2.9 \times 10^{18}$ (cm^{-3} s^{-1}) and different photon densities ρ, initial photosensitizer concentrations $[S_0]_i$ and oxygen parameters. From (a) to (d): $\rho_1 = 2.0 \times 10^6$ (cm^{-3}), $\rho_2 = 7.0 \times 10^6$ (cm^{-3}), $\rho_3 = 2.0 \times 10^7$ (cm^{-3}), $[S_0]_i = 7.0 \times 10^{13}$ (cm^{-3}). For (e) and (f): $[S_0]_{i1} = 1.0 \times 10^{15}$ (cm^{-3}), $[S_0]_{i2} = 7.0 \times 10^{12}$ (cm^{-3}), $[S_0]_{i3} = 1.0 \times 10^{12}$ (cm^{-3}), $\rho = 5.0 \times 10^6$ (cm^{-3}). Other parameters in (e) and (f) are the same as those in (a) except the following: (f) $D = 8 \times 10^{-7}$ (cm^2 s^{-1}), $D' = 2 \times 10^{-6}$ (cm^2 s^{-1}). All other coefficients are given in the Appendix. Each set of curves marked with either ρ or $[S_0]_i$ consists of three lines calculated at different cell locations: solid: $r = 0$; dot: $r = r_0/2$ and dash: $r = r_0$.
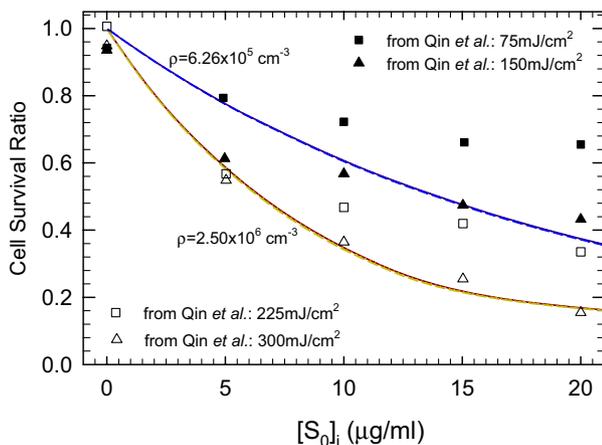
Figure 8. Comparison of two calculated cell survival curve sets with the measured data represented by the symbols by Qin *et al.* (5). All parameters used in the numerical calculations are the same as those in Fig. 7(a) except the following: $\beta_0 = 8.0 \times 10^{-2}$ (s^{-1}) and $[^3O_2]_I = 4.0 \times 10^{17}$ (cm^{-3}). Note that the photon density $\rho = 6.25 \times 10^5$ and 2.50×10^6 (cm^{-3}) corresponds respectively to fluence $F = 75$ and 300 (mJ cm^{-2}) while $[S_0]_i = 4.0 \times 10^{12}$ (cm^{-3}) corresponds to 20 (μg mL^{-1}) using the molecular mass of Photofrin® as 3000 (g mol^{-1}). Each set of curves marked with ρ consists of three lines calculated at different cell locations: solid: $r = 0$; dot: $r = r_0/2$ and dash: $r = r_0$.

values of $[^3O_2]_i$ and β_0 from those used in Fig. 8(a). For the lower fluence case the model overestimates the cell killing, which could be attributed to the use of homogeneous and spherical cell configuration and/or the lack of sufficient account of cell repair mechanisms. Despite this deficiency, one can still see that the present model provides an efficient and powerful tool to quantitate the dependence of cell survival ratios on various parameters of light, photosensitizer and oxygen for *in vitro* cell studies by Type-II PDT.

CONCLUSION

In this report, we presents a significantly improved model of Type-II PDT by including oxygen transport and a quantitative description of cell killing using a spherical cell configuration over the previous efforts by other researchers (7–9) and us. A group of differential equations with appropriate boundary conditions is developed to simulate the time evolution of key molecule concentrations and oxygen transport as a coupled system. This allows us to extract the decay constants of photosensitizer S_0 and oxidized receptors R to quantitate the photobleaching and cytotoxicity related PDT within the ranges of experimentally controllable parameters of $[S_0]_i$ and ρ with

different oxygen and transport parameters. The consistency of the equation group is examined by determination of the conditions for obtaining nonnegative concentrations. In addition, the present model includes a cell killing equation in which the excited singlet oxygen is used as the representative molecules of ROS and linked to the cell killing rates through two different pathways. Using this model one can calculate the cell survival curves from the concentrations of unoxidized receptors $[R]$ and the singlet oxygen molecules $[^1O_2]$ representing the ROS stress. More important, the modeling results can be compared directly to the experimental results based on the measurement of oxygen or singlet oxygen concentrations and cell survival ratios or used for design of different *in vitro* studies of PDT. Thus, the new model has the capacity to be used as a platform to study *in vitro* the complex molecular interactions leading to cell killing by Type-II PDT in the presentation of oxygen transport. Further improvement of this model for detailed analysis of cell killing through PDT can be achieved by considering the molecular pathways underlying cell death and repair and heterogeneous distribution of the target sites in the cell.

APPENDIX

The following coefficients are used to solve the differential equations, their sources were given in table 1 of reference (7) unless noted otherwise.

Light speed in tissue: $v = 2.17 \times 10^{10}$ (cm s^{-1});

Cross-section of light absorption of cells containing S_0: $\sigma_{psa} = 5.0 \times 10^{-13}$ (cm^2);

Relaxation time of S_1 to S_0: $\tau_1 = 10$ ns;

Relaxation time of T to S_0: $\tau_3 = 30$ μs;

Relaxation time of $^1O_2$ to $^3O_2$: $\tau_0 = 30$ ns;

Quantum yield of S_1 transition to S_0: $\eta_{10} = 0.20$;

Quantum yield of S_1 intersystem crossing to T: $\eta_{13} = 0.80$;

Quantum yield of T transition to S_0: $\eta_{30} = 0.30$;

Efficiency factor for energy transfer from T to $^3O_2$: $\alpha_s = 1 \times 10^{-17}$ (cm^3)

Quantum yield of $^1O_2$ transition to $^3O_2$: $\eta_0 = 0.30$;

Photobleaching rate: $k_{pb} = 2.0 \times 10^{-10}$ (cm^{3}s^{-1});

Cytotoxicity rate: $k_{cx} = 2.0 \times 10^{-9}$ (cm^{3}s^{-1});

Scavenging rate: $k_{sc} = 1.0 \times 10^{-9}$ (cm^{3}s^{-1});

Initial concentration of oxygen scavengers: $[C]_i = 1.0 \times 10^3$ (cm^{-3});

Michaelis constant for oxygen uptake: $K_m = 1.5 \times 10^{17}$ (cm^{-3}; 19);

Initial concentration of unoxdized receptors: $[R]_i = 5.0 \times 10^{17}$ (cm^{-3});

Rate coefficient of cell killing by oxidized receptors: $\beta_0 = 1.0 \times 10^{-2}$ (s^{-1}) or 8.0×10^{-2} (s^{-1});

Maximum rate of cell killing by single oxygen: $V_c = 4.0 \times 10^{-3}$ (cm^{-3}s^{-1});

Michaelis constant for singlet oxygen uptake in cell killing: $K_c = 2.0 \times 10^9$ (cm^{-3}).

In addition to the above coefficients, a parameters of photon density ρ (cm^{-3}) is employed in Eq. (1) to represent the incident light flux as $v\rho$ over the illuminated cells and can be related to the fluence F as $F = 4 \times 10^{-9}\rho t$.

REFERENCES

1. Allison, R. R., G. H. Downie, R. Cuenca, X. H. Hu, C. J. H. Childs and C. Sibata (2004) Photosensitizers in clinical PDT. *Photodiagn. Photodyn. Ther*. **1**, 27–42.
2. Agostinis, P., K. Berg, K. A. Cengel, T. H. Foster, A. W. Girotti, S. O. Gollnick, S. M. Hahn, M. R. Hamblin, A. Juzeniene, D. Kessel, M. Korbelik, J. Moan, P. Mroz, D. Nowis, J. Piette, B. C. Wilson and J. Golab (2011) Photodynamic therapy of cancer: an update. *CA Cancer J. Clin*. **61**, 250–281.
3. Sporn, L. A. and T. H. Foster (1992) Photofrin and light induces microtubule depolymerization in cultured human endothelial cells. *Cancer Res*. **52**, 3443–3448.
4. Dysart, J. S. and M. S. Patterson (2005) Characterization of Photofrin photobleaching for singlet oxygen dose estimation during photodynamic therapy of MLL cells *in vitro*. *Phys. Med. Biol*. **50**, 2597–2616.
5. Qin, Y., D. Xing, S. Luo, J. Zhou, X. Zhong and Q. Chen (2005) Feasibility of using fluoresceinyl Cypridina luciferin analog in a novel chemiluminescence method for real-time photodynamic therapy dosimetry. *Photochem. Photobiol*. **81**, 1534–1538.
6. Hilf, R. (2007) Mitochondria are targets of photodynamic therapy. *J. Bioenerg. Biomembr*. **39**, 85–89.
7. Hu, X. H., Y. Feng, J. Q. Lu, R. R. Allison, R. E. Cuenca, G. H. Downie and C. H. Sibata (2005) Modeling of a Type II photofrin-mediated photodynamic therapy process in a heterogeneous tissue phantom. *Photochem. Photobiol*. **81**, 1460–1468.
8. Foster, T. H., R. S. Murant, R. G. Bryant, R. S. Knox, S. L. Gibson and R. Hilf (1991) Oxygen consumption and diffusion effects in photodynamic therapy. *Radiat. Res*. **126**, 296–303.
9. Georgakoudi, I., M. G. Nichols and T. H. Foster (1997) The mechanism of Photofrin photobleaching and its consequences for photodynamic dosimetry. *Photochem. Photobiol*. **65**, 135–144.
10. Gkigkitzis, I., C. Yang, Y. Feng, J. Q. Lu and X. H. Hu (2011) Modeling of PDT kinetics in cell killing. *Proc. SPIE* **7886**, 78860O.
11. Moor, A. C. (2000) Signaling pathways in cell death and survival after photodynamic therapy. *J. Photochem. Photobiol*. **57**, 1–13.
12. Sod, G. A. (1986) A numerical study of oxygen diffusion in a spherical cell with the Michaelis–Menten oxygen uptake kinetics. *J. Math. Biol*. **24**, 279–289.
13. King, M. R. (2004) Apparent 2-D diffusivity in a ruffled cell membrane. *J. Theor. Biol*. **227**, 323–326.
14. Massaro, T. A. and I. Fatt (1969) Oxygen diffusion in large single-celled organisms. *Bull. Math. Biophys*. **31**, 327–340.
15. Belousova, I. M., N. G. Mironova and M. S. Yur'ev (2005) A mathematical model of the photodynamic fullerene-oxygen action on biological tissues. *Opt. Spectrosc*. **98**, 349–356.
16. Pelicano, H., D. Carney and P. Huang (2004) ROS stress in cancer cells and therapeutic implications. *Drug Resist. Updat*. **7**, 97–110.
17. Evans, L. C. (2010) A strong maximum principle for parabolic systems in a convex set with arbitrary boundary. *Proc. Amer. Math. Soc*. **138**, 3179–3185.
18. McElwain, D. L. (1978) A re-examination of oxygen diffusion in a spherical cell with Michaelis–Menten oxygen uptake kinetics. *J. Theor. Biol*. **71**, 255–263.
19. McElwain, D. L., R. Callcott and L. E. Morris (1979) A model of vascular compression in solid tumours. *J. Theor. Biol*. **78**, 405–415.